6th European Conference on Computational Mechanics (ECCM 6)
7th European Conference on Computational Fluid Dynamics (ECFD 7)
1115 June 2018, Glasgow, UK

EFFICIENT SOLID SHELL ELEMENT FOR THE COUPLED THERMO-MECHANICAL STABILITY ANALYSIS OF THIN-WALLED STRUCTURES

Wenya Shu[1] and Ilinca Stanciulescu[2]*

[1] Rice University, Department of Civil and Environmental Engineering, 6100 Main St, Houston, TX, USA, ws18@rice.edu

[2] Rice University, Department of Civil and Environmental Engineering, 6100 Main St, Houston, TX, USA, ilinca.s@rice.edu

Key words: Solid-shell, Isothermal scheme, Implicit, Analytical mass

Abstract. We propose an efficient and robust coupled thermo-mechanical solid shell formulation to enable the stability analysis of thin-walled structures. Of particular interest is the ability to study the snap through behavior of panels subjected to a combined thermo-mechanical environment. Three classical techniques, the assumed natural strain (ANS) interpolation, the enhanced assumed strain (EAS) method and reduced integration with hourglass control are employed to avoid locking and improve convergence [1]. Although previous studies demonstrated that the solid shell element incorporating these techniques performs well in static and explicit transient analysis, few of them discussed the element performance in conducting transient analysis using implicit time integration. We propose an analytical evaluation of the mass matrix, which guarantees both accurate and efficient implicit transient analysis. Finally, the formulation is extended to include thermo-mechanical coupling using the isothermal staggered scheme. Numerical examples demonstrate the accuracy of the present element in both mechanical transient and thermo-mechanical stability analyses. The present element is robust in long-duration time history large deformation simulations and is several times more efficient than the standard quadratic solid element.

1 INTRODUCTION

In areospace engineering, thin-walled structures are widely used and often experience instablility (e.g., snap-through) when subjected to mechanical forces and thermal loads. The accurate analysis of the thermo-mechanical coupled problem demands a reliable and robust finite element formulation. The quadratic solid element was implemented to conduct thermo-mechanical stability simulation in [1]. The quadratic element is accurate but leads to very inefficient modeling. The low-order solid element has superior efficiency in the detailed modeling but is prone to locking in simulations of bending or incompressibility.

The development of solid-shell elements for the analysis of thin-walled structures has been of interest for decades. Numerous articles discussed effective treatments to avoid locking effects associated with the solid-shell element. The combination of enhanced strain method (EAS) and assumed natural strain method (ANS) is demonstrated to be very effective in removing the locking of the solid-shell element (e.g., [2,3]). A very efficient Reduced Enhanced Solid Shell (RESS) element applied the reduced integration concept with the EAS method was proposed in [4]. Cardoso et al. [5] and Schwarze and Reese [6] further improved the accuracy and stability of the RESS element.

Recent decades also witnessed increased interests in the development of the solid-shell element for transient analysis. Incorporating ANS and EAS locking treatments, a solid-shell element for transient analysis in conjunction with implicit time integration was developed in [7,8]. The solid-shell element accommodating explicit dynamic modeling was also studied in [9,10]. Particularly, [9] showed that the solid shell element proposed in [6] can be used for the efficient explicit analysis. Despite these extensive studies on solid-shell elements, the behavior of the reduced integration solid-shell element in transient analysis using implicit time integration is not yet reported in any other literature.

To solve the fully coupled thermo-mechanical system, monolithic and staggered split schemes are often adopted. A monolithic algorithm applies the same time integrator to the whole system and solves the two fields simultaneously. Monolithic schemes can achieve unconditional stability with implicit time-stepping algorithms [11]. However, they result into large, non-symmetric systems. Staggered algorithms result in two reduced and symmetric systems (one for each of the two different fields) that can be solved independently. For example, the isothermal scheme consists of a isothermal mechanical phase followed by a heat conduction phase with constant configuration.

In this work, an isothermal staggered solid-shell element for efficient thermo-mechanical coupled analysis of thin-walled structures is presented. Numerical examples are included to demonstrate the performance of the solid-shell element in capturing complex dynamic behaviors of structures and conducting thermo-mechanical stability analysis.

2 FINITE ELEMENT FORMULATION

Based on the isothermal staggered scheme, element formulations in mechanical and thermal fields are presented separately. Locking free techniques are empolyed to eliminate locking effects in conducting mechanical analysis. In the thermal field, the solid-shell element is similar to the conventional 8-node solid element with full integration.

2.1 Mechanical phase

Let us consider a continuum body in motion subjected to surface loads $\mathbf{t}$ and body forces $\rho_0\mathbf{b}$. For the EAS method with the orthogonality assumption between the enhanced strain and stress fields ($\int_V \mathbf{S} : \mathbf{E}^{eh} dV = 0$), the continuous weak form is

$$\delta\Pi(\mathbf{u}, \mathbf{E}^{eh}) = \int_\Omega \mathbf{S} : \delta(\mathbf{E}^c + \mathbf{E}^{eh}) dV + \int_\Omega \delta\mathbf{u}\cdot\rho_0\ddot{\mathbf{u}} dV - \int_\Omega \delta\mathbf{u}\cdot\rho_0\mathbf{b} dV - \int_\Gamma \delta\mathbf{u}\cdot\mathbf{t} d\Gamma = 0 \quad (1)$$

Note that isothermal staggered scheme solves the mechanical phase with constant tem-

perature. Thus, the variation with respect to temperature(θ) is unnecessary in the mechanical phase. Equation 1 is discretized in space with the eight node solid-shell element. The tri-linear shape function used for the isoparametric representations can be written in the following polynomial form

$$N_I = 1/8(1 + g_1^I\xi + g_2^I\eta + g_3^I\zeta + h_1^I\xi\eta + h_2^I\eta\zeta + h_3^I\xi\zeta + h_4^I\xi\eta\zeta) \tag{2}$$

where g_1^I, g_2^I, g_3^I, h_1^I, h_2^I, h_3^I, h_4^I (with I=1,...,8) represent coefficients of the shape function at the node I.

The in-plane one-point reduced quadrature [4] and the modified ANS method [5] are also incorporated to relieve the locking effect. To stabilize the singular stiffness matrix induced by the reduced integration, Schwarze and Reese [6] defined the hourglass strain with deviatoric character. Following those locking free techniques and transforming the Green-Lagrange strain from convective coordinates to Cartesian coordinates with the polynomial approximation of the transformation matrix, the strain can be represented by

$$\mathbf{E}^c \approx \overbrace{\mathbf{E}^{c0} + \zeta\mathbf{E}^{c\zeta} + \zeta^2\mathbf{E}^{c\zeta\zeta}}^{\mathbf{E}^{c\star}} + \overbrace{\xi\mathbf{E}^{c\xi}_{dev} + \eta\mathbf{E}^{c\eta}_{dev} + \xi\zeta\mathbf{E}^{c\xi\zeta}_{dev} + \eta\zeta\mathbf{E}^{c\eta\zeta}_{dev}}^{\mathbf{E}^{chg}} \tag{3}$$

Inserting the variation of the displacement and strain in the matrix forms ($\delta\mathbf{u} = \mathbf{N_u}\delta\mathbf{u}^e$, $\delta\mathbf{E}^c = \mathbf{B}^c\delta\mathbf{u}^e$ and $\delta\mathbf{E}^{eh} = \mathbf{B}^{eh}\delta w^e$) and solving the mechanical phase in reference configuration, the discrete weak form at the element level can be written as

$$\begin{aligned}\delta\Pi(\mathbf{u^{(e)}}, w^{(e)}) &= \delta\mathbf{u}^{eT}\Big\{\int_{\Omega_e}\mathbf{N_u}^T\rho_0\mathbf{N_u}dV\ddot{\mathbf{u}}^e + \int_{\Omega_e}\mathbf{B}^{cT}\mathbf{S}dV - \int_{\Omega_e}\mathbf{N_u}^T\rho_0\mathbf{b}dV - \int_{\Gamma_e}\mathbf{N_u}^T\mathbf{t}d\Gamma\Big\} \\ &+ \delta w^e\int_{\Omega_e}\mathbf{B}^{ehT}\mathbf{S}dV = \mathbf{0}\end{aligned} \tag{4}$$

To apply the Newton-Raphson method, the discrete form needs to be further linearized as follows

$$\begin{cases}\mathbf{M}\Delta\ddot{\mathbf{u}}^\mathbf{e} + \mathbf{K}^e_{uu}\Delta\mathbf{u}^\mathbf{e} + \mathbf{K}^e_{uw}\Delta w^e = \mathbf{f}^e_{ext} - \mathbf{f}^e_{int} - \mathbf{f}^e_{mass} \\ \mathbf{K}^{e\ T}_{uw}\Delta\mathbf{u}^e + K^e_{ww}\Delta w^e = -f^e_{EAS}\end{cases} \tag{5}$$

Introducing the assumption that the infinitesimal volume element $dV_e = Jd\Omega_e = J^0d\Omega_e$ ($J^0 = det(J|_{\xi=\mathbf{0}})$) and considering in-plane reduced integration, stiffness matrices and residue vectors take the following simplified forms

$$\mathbf{f}^e_{int} = \int_{\Omega_e}\mathbf{B}^{chgT}_{dev}\mathbf{C}^{hg}\mathbf{E}^{chg}_{dev}dV + \int_{-1}^{1}\mathbf{B}^{c\star T}\mathbf{S}^\star d\zeta 4J^0 \quad and \quad f^e_{EAS} = \int_{-1}^{1}\mathbf{B}^{ehT}\mathbf{S}^\star d\zeta 4J^0$$

$$\mathbf{K}^e_{uw} = \int_{-1}^{1}\mathbf{B}^{c\star T}\mathbf{C}\mathbf{B}^{eh}d\zeta 4J^0 \quad and \quad K^e_{ww} = \int_{-1}^{1}\mathbf{B}^{ehT}\mathbf{C}\mathbf{B}^{eh}d\zeta 4J^0$$

$$\mathbf{K}^e_{uu} = \int_{\Omega_e}\big\{\mathbf{B}^{chgT}_{dev}\mathbf{C}^{hg}\mathbf{B}^{chg}_{dev} + \mathbf{G}^{chgT}_{dev}\mathbf{C}^{hg}\mathbf{E}^{chg}_{dev}\big\}dV + \int_{-1}^{1}\big\{\mathbf{B}^{c\star T}\mathbf{C}\mathbf{B}^{c\star} + \mathbf{G}^{c\star T}\mathbf{S}^\star\big\}d\zeta 4J^0$$

Where $\mathbf{G}^c$ is used for computing the geometric stiffness matrices and can be obtained by $\frac{\partial\mathbf{B}^c}{\partial\mathbf{u}^e}$. Note that the matrices and vectors related to hourglass control can be calculated analytically. For details, the reader is referred to [6].

The lumped mass and the consistent mass are defined as $\mathbf{M}_{IJ}^{Lump} = \int_V \rho_0 N_I dV \delta_{IJ} \mathbf{I_{3\times 3}}$ and $\mathbf{M}_{IJ}^{Cons} = \int_V N_I \rho_0 N_J dV \mathbf{I_{3\times 3}}$ respectively to accommodate the transient analysis. The analytical expressions for the mass matrix terms are given by

$$M_{IJ}^{Lump} = 8J^0 \rho_0 r_I \delta_{IJ} \tag{6}$$

$$M_{IJ}^{Cons} = 8J^0 \rho_0 \big\{ r_I r_J + \frac{1}{3}(g_1^I g_1^J + g_2^I g_2^J + g_3^I g_3^J) + \frac{1}{9}(h_1^I h_1^J + h_2^I h_2^J + h_3^I h_3^J) + \frac{1}{27} h_4^I h_4^J \big\} \tag{7}$$

Prior to assembly of the global matrices, the EAS parameter increment Δw^e can be solved at the element level by using static condensation. Applying the Hilber-Hughes-Taylor (HHT-α) time integrator [12] to solve the dynamic system, the tangent and the residual corresponding to the Newton Raphson's method are given by

$$\mathbf{K}_T^e = \frac{1}{\beta \Delta t^2} \mathbf{M}^e + \alpha [\mathbf{K}_{uu}^e - \mathbf{K}_{uw}^e (K_{ww})^{-1} \mathbf{K}_{uw}^{e\ T}] \tag{8}$$

$$\mathbf{R^e} = \mathbf{f}_{ext}^e - \mathbf{f}_{int}^e - \mathbf{f}_{mass}^e + \mathbf{K}_{uw}^e (K_{ww})^{-1} f_{EAS}^e \tag{9}$$

The above general form reduces to the classical Newmark algorithm for $\alpha = 1$.

2.2 Thermal phase

The strong form governing equation for the thermal phase according to the first principle of thermodynamics is

$$\rho_0 \dot{\eta} + \nabla \cdot \mathbf{Q} = R \tag{10}$$

$$\mathbf{Q} = -Jk\mathbf{F}^{-1}\mathbf{F}^{-T}\nabla_{\mathbf{X}}\theta \tag{11}$$

where η is the specific entropy, θ is the temperature, $\mathbf{Q}$ is the heat flux in the reference configuration, R defines the external heat source, $\mathbf{F}$ is the deformation gradient and J=det($\mathbf{F}$).

We use the St.Venant-Kirchhoff material model and the Helmholtz free energy Ψ given as

$$\Psi = \frac{1}{2}[\lambda (tr\mathbf{E})^2 + 2\mu \mathbf{E} : \mathbf{E}] - 3\kappa\alpha(\theta - \theta_0) tr\mathbf{E} + \rho_0 c_v (\theta - \theta_0 - \theta log\frac{\theta}{\theta_0}) \tag{12}$$

where θ_0 is the ambient temperature, α defines as thermal expansion coefficient and the bulk modulus κ can be represented by the Lam*é* parameters as $\kappa = \lambda + 2\mu/3$.

Given that the entropy is defined as

$$\eta = -\frac{\partial \Psi}{\rho_0 \partial \theta} = \frac{3\kappa\alpha}{\rho_0} tr\mathbf{E} + c_0 \frac{\theta}{\theta_0} \tag{13}$$

the governing equation (10) can be rewritten as

$$\rho_0 c_v \dot{\theta} + 3\kappa\alpha\theta tr\dot{\mathbf{E}} + \nabla \cdot \mathbf{Q} = R \tag{14}$$

The weak form in the reference domain becomes

$$\int_\Omega \delta\theta \rho_0 c_v \dot{\theta} dV + \int_\Omega \delta\theta 3\kappa\alpha tr\dot{\mathbf{E}}\theta dV - \int_\Omega (\nabla\delta\theta) \cdot \mathbf{Q} dV + \int_\Gamma \delta\theta Q_n d\Gamma - \int_\Omega \delta\theta R dV = 0 \tag{15}$$

According to the isothermal scheme, the thermal problem is solved at fixed configuration. Thus, Eq. 15 is only linearized with respect to temperature θ in the reference configuration. We further push the problem forward to solve in the current configuration. The linearized discrete form of the thermal equation at the element level is obtained as

$$\begin{aligned} &\int_{\Omega_e} \mathbf{N}_\theta \rho c_v \mathbf{N}_\theta dv \Delta\dot{\theta} + \int_{\Omega_e} \mathbf{N}_\theta \frac{3\kappa\alpha}{J} tr\dot{\mathbf{E}} \mathbf{N}_\theta dv \Delta\theta + \int_{\Omega_e} \mathbf{B}_\theta^{\mathbf{T}} k \mathbf{B}_\theta dv \Delta\theta \\ = &\int_{\Omega_e} \mathbf{N}_\theta r dv - \int_{\Gamma_e} \mathbf{N}_\theta q_n d\Gamma - \int_{\Omega_e} \mathbf{N}_\theta \rho c_0 \dot{\theta} dv - \int_{\Omega_e} \mathbf{N}_\theta \frac{3\kappa\alpha}{J} tr\dot{\mathbf{E}} \theta dv - \int_{\Omega_e} \mathbf{B}_\theta^{\mathbf{T}} k \nabla_x \theta dv \end{aligned} \tag{16}$$

where N_θ is the same as Eq. 2 and $\mathbf{B}_\theta = \frac{\partial \mathbf{N}_\theta}{\partial \mathbf{x}}$. Full integration quadrature is adopted to obtain all matrices numerically. The backward Euler method is employed to solve the equation.

3 NUMERICAL EXAMPLES

The finite element formulation presented above for the isothermal staggered analysis has been implemented into the Finite Element Analysis Program (FEAP) [13]. In this section, we demonstrate the robustness and accuracy of the element implementation in capturing complex system behaviors of thin-walled structures.

3.1 Dynamic buckling of the hinged cylindrical panel

In this section, we consider a cylindrical panel with hinged longitudinal edges and free circumferential edges. The geometry is described by radius $R = 2540$ mm, angle of the circumferential edge $\theta = 0.2$ rad, length of the longitudinal edge $L = 508$ mm and panel thickness $t = 12.7$ mm. The material is prescribed to be elastic isotropic with $E = 310.275$ MPa and $\nu = 0.3$. A total of 256 (16×8×2) elements are used to discretize the panel. Two layers of elements through the thickness allow for easy consideration of the hinged boundary conditions. A downward ramp load with $P_0 = 400$N and $t_0 = 0.01$s (see Fig. 1(a)) is applied at the panel center. The Newmark time integrator with time step $\Delta t = 0.001$s was used. Simulations using consistent and lumped mass are performed respectively.

Figure 1(b) compares the time history of the displacement at the panel center obtained from the present analyses with the numerical result in [14]. For both consistent and lumped mass, good agreement between the present analyses and the reference solution is obtained.

3.2 Dynamic buckling of a fully clamped spherical cap

We investigate the dynamic behavior of a spherical cap under a concentrated apex load in this example. The geometry of the spherical cap is given by the radius of curvature $R = 120.904$ mm, base radius $a = 22.86$ mm, thickness $t = 0.400304$ mm (Fig. 2(a)). The material is assumed to be linear elastic with Young's modulus $E = 68948$ MPa, Poisson ratio $\mu = 0.3$, and density $\rho = 2620$ kg/m^3. As shown in Fig. 2(b), a concentrated load $P = 445$ N is applied at the apex instantly and lasts for a duration of 500 μs.

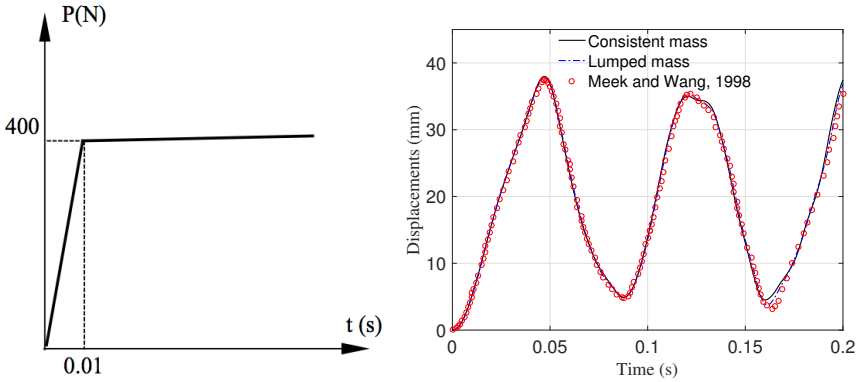

(a) Step load (b) Time history of the center displacement

Figure 1: Load and response of the cylindrical panel

Taking advantage of the axisymmtric configuration and loading condition, [15] analyzed this problem with the 8-node axisymmetric element. In this study, we mesh the cap with 896 elements with only one layer of elements through thickness. The cap is fully clamped at the base.

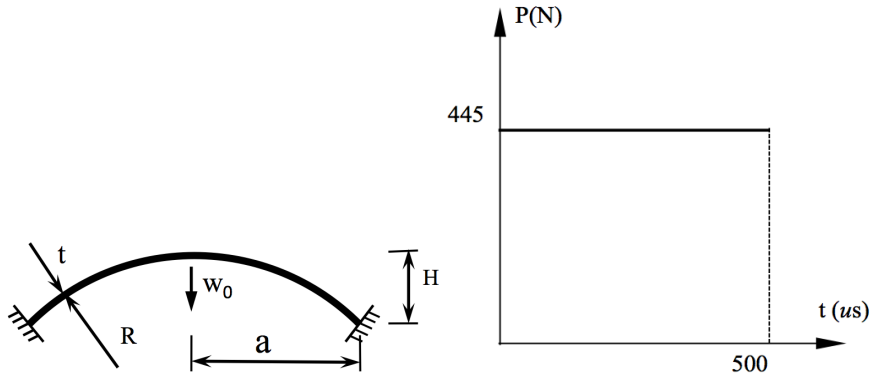

(a) Spherical cap (b) Step load for the spherical cap

Figure 2: Spherical cap subjected to a step load

The transient problem is solved using Newmark's algorithm and time step $\Delta t = 2\mu$s. Fig. 3 plots the time history of the ratio between the displacement at the apex (W_0) and the cap height (H). The results of the present study agree well with the reference result reported by [15]. The influence of lumped mass vs. consistent mass on the dynamic response is also investigated. As shown in Fig. 3, the result given by the lumped mass is closer to the reference solution than the one obtained using the consistent mass. This might be due to the fact the reference result was based on the lumped mass idealization in [15].

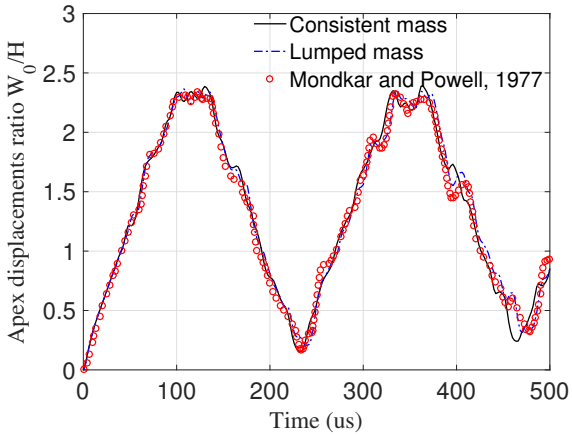

Figure 3: Dynamic response of the spherical cap

3.3 Vibration of the pinched hemispherical shell

A recent study [16] reveals more details of dynamic analysis of the classical pinched hemispherical shell problem and is followed here to examine the performance of the present solid-shell element. The hemispherical shell has an 18° hole at the top, and is subjected to a pair of inward and a pair of outward forces at the free edge with 90° apart. A time dependent load shown in Fig. 4(a) is the same as in [16]. The geometry parameters are radius $R = 10$, thickness $h = 0.04$. The material is assumed to be linear elastic with $E = 6.825 \times 10^7$, $\nu = 0.3$ and density $\rho = 0.001$.

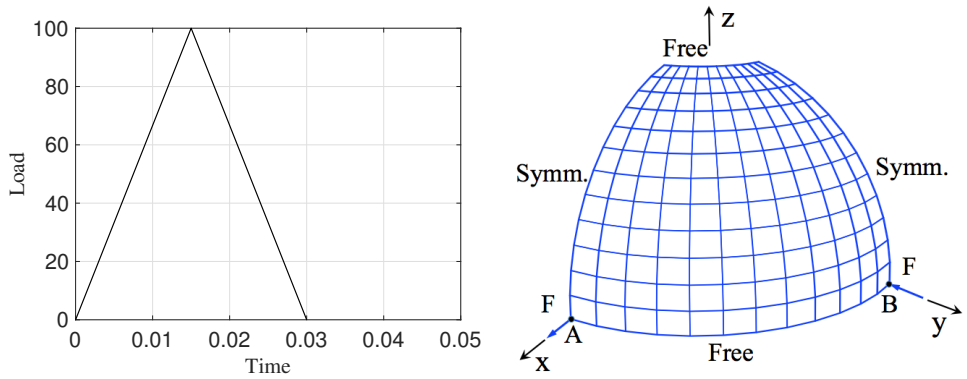

(a) Time dependent load (b) One quadrant of sperical shell

Figure 4: Hemispherical shell subjected to pinch load

Due to symmetry, only one quarter of the shell is meshed (Fig. 4(b)). The HHT$-\alpha$ time integrator with $\alpha = 0.995$ is applied to avoid numerical instability. Every simulation was run for 5000 steps using the step size $\Delta t = 0.0002$. As shown in Fig. 5, the displacement histories of point A and B are compared to the reference solutions. The comparisons show that even the relatively coarse mesh with $12 \times 12 \times 1$ elements gives very close results to

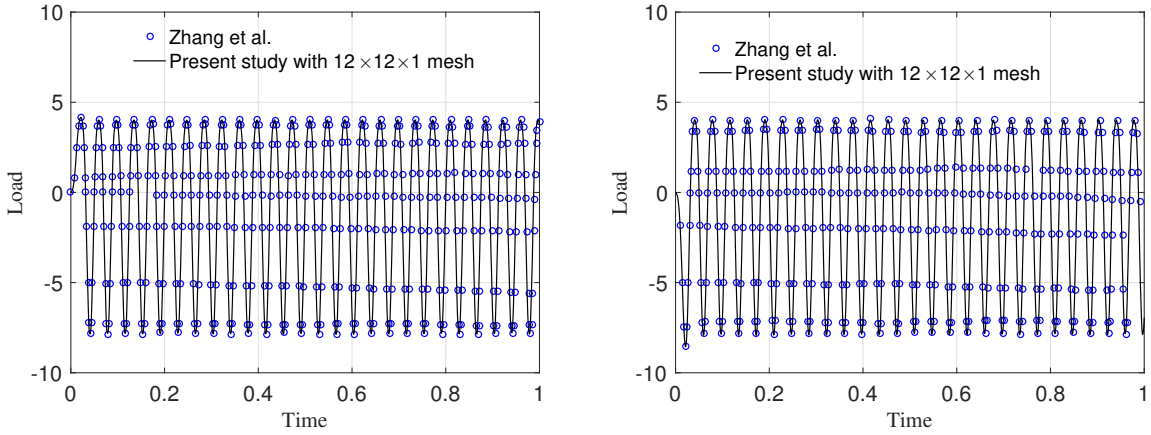

(a) U_x of point A (b) U_y of point B

Figure 5: Displacement history of point A and B

the reference solutions obtained with a mesh with 16×16 shell elements in [16].

3.4 Thermo-mechanical snap-through of the shallow arch

The transient simulation of the structure undergoing snap-through is very challenging due to the high non-linearity and potential loss of stability. Thus, the thermo-mechanical modeling of the snap-through is an ideal test example to evaluate the robustness of the present solid-shell element in long-duration time history analyses. A shallow arch with two ends fully clamped is considered in this example (Fig. 6). The arch has radius R=180 in., span a = 12 in., transverse width w = 0.5 in. and thickness t = 0.04 in. The material is assumed to be elastic isotropic with E = 206483 MPa, $\nu = 0.28$, $\rho = 7834$ kg/m^3, thermal expansion coefficient $\alpha = 1.5 \times 10^{-5} K^{-1}$, specific capacity $c_v = 460\ \frac{J}{kg \cdot K}$ and conductivity $\kappa = 45$ N/sK. The reference temperature is defined as 300 K.

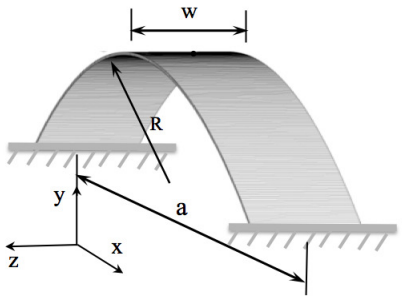

Figure 6: Shallow arc illustration

We perform two simulations with the same harmonic load $F = 2.9 \sin(188\pi t)$ at the midpoint but different initial temperatures of 290 K and 315 K respectively. All arch surfaces are assumed to be insulated. In the isothermal staggered scheme, the HHT-α

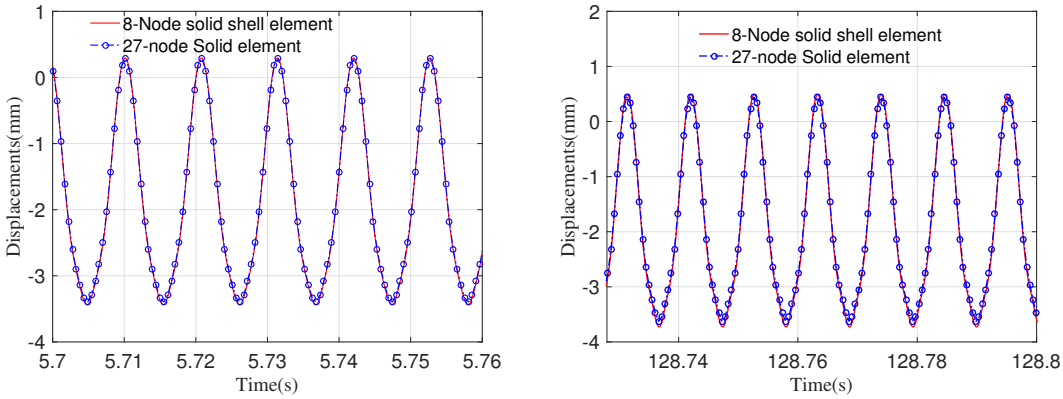

(a) T=290K (b) T=315K

Figure 7: Time history of the displacement at the steady state

time integrator with $\alpha = 0.99$ is applied to solve the mechanical phase and the backward Euler method is used to solve the thermal phase. The simulation is conducted with the time step $\Delta t = 1/(94 \times 200)$. All simulations are run until steady state is reached so that we can safely exclude the possibility that the snap-through is the result of short-term transient effects.

Fig. 7 shows the time history of the displacement corresponding to the the steady state response. For comparison, all simulations are repeated using 27-node solid elements. It is clearly revealed that the shallow arch undergoes periodic persistent snap-through in both scenarios. The investigation also suggests that the present element can bring more than 80% reduction in the computational time to achieve the same accuracy as the 27-node solid element. We can thus remark that the proposed solid-shell element can handle the thermo-mechanical snap through modeling accurately and efficiently.

4 CONCLUSIONS

This paper presents an efficient eight-node solid-shell element for the thermo-mechanical stability modeling of thin-walled structures. The isothermal staggered scheme is adopted to solve the fully coupled system. To avoid locking, three effective locking-free techniques are incorporated. We proposed an analytic method to calculate the mass matrix and inertial term for an accurate and efficient transient analysis using implicit time integration. Assuming fixed configuration, the thermal analysis is conducted by using the conventional 8-node thermal solid element with full integration.

The present element is locking-free in both the mechanical and the thermo-mechanical analysis of thin-walled structures. Numerical examples confirm that the element is accurate in predicting complex structural responses in transient analyses with implicit time integration. The most striking feature of the present solid-shell element is the capability to capture steady state response exactly, while also allowing for a 80% reduction of computational time comparing with the quadratic solid element in the thermo-mechanical

coupled analysis.

REFERENCES

[1] Stanciulescu, I., Mitchell, T. and Chandra, Y. et al., A lower bound on snap-through instability of curved beams under thermomechanical loads. *International Journal of Non-Linear Mechanics* (2012) **47**:561-575.

[2] Klinkel, S. and Gruttmann, F. and Wagner W., A continuum based three-dimensional shell element for laminated structures. *Computers & Structures* (1999) **71**:43-62.

[3] Vu-Quoc, L. and Tan, X.G., Optimal solid shells for non-linear analyses of multilayer composites. I. Statics. *Computer methods in applied mechanics and engineering* (2003) **71**:975-1016.

[4] Alves de Sousa, R.J., Cardoso, R.P., Fontes Valente, R.A., et al., A new one-point quadrature enhanced assumed strain (EAS) solid-shell element with multiple integration points along thickness: Part I-geometrically linear applications. *International journal for numerical methods in engineering* (2005) **62**:952-977.

[5] Cardoso, R.P., Yoon, J.W., Mahardika, M., et al., Enhanced assumed strain (EAS) and assumed natural strain (ANS) methods for one-point quadrature solid-shell elements. *International journal for numerical methods in engineering* (2008) **75**:156-187.

[6] Schwarze, M and Reese, S., A reduced integration solidshell finite element based on the EAS and the ANS concept:Large deformation problems. *International journal for numerical methods in engineering* (2008) **85**:289-329.

[7] Vu-Quoc, L. and Tan, X.G., Optimal solid shells for non-linear analyses of multilayer composites. II. Dynamics. *Computer Methods in Applied Mechanics and Engineering* (2003) **192**:1017 - 1059.

[8] Hajlaoui, A., Triki, E. and Frikha A. et al. Nonlinear Dynamics Analysis of FGM Shell Structures with a Higher Order Shear Strain Enhanced Solid-Shell Element. *Latin American Journal of Solids and Structures* (2017) **14**:72-91.

[9] Pagani, M. and Reese, S. and Perego, U., Computationally efficient explicit nonlinear analyses using reduced integration-based solid-shell finite elements. *Computer Methods in Applied Mechanics and Engineering* (2014) **268**:141-159.

[10] Mattern, S. and Schmied, C. and Schweizerhof, K., Highly efficient solid and solid-shell finite elements with mixed strain–displacement assumptions specifically set up for explicit dynamic simulations using symbolic programming. *Computers & Structures* (2015) **154**:210-225.

[11] Armero, F. and Simo, J.C., A new unconditionally stable fractional step method for non-linear coupled thermomechanical problems. *International Journal for Numerical Methods in Engineering* (1992) **35**:737–766.

[12] Hilber, H.M., Hughes, T.J. and Taylor, R.L., Improved numerical dissipation for time integration algorithms in structural dynamics. *Earthquake Engineering & Structural Dynamics* (1977) **5**:283–292.

[13] Taylor, R.L. and Govindjee S., Feap–a finite element analysis program. *Version 8.5 Programmer Manual* (2017).

[14] Meek, J.L. and Wang, Y., Nonlinear static and dynamic analysis of shell structures with finite rotation. *Computer Methods in Applied Mechanics and Engineering* (1998) **162**:301 - 315.

[15] Mondkar, D.P. and Powell, G.H., Finite element analysis of non-linear static and dynamic response. *International Journal for Numerical Methods in Engineering* (1977) **11**:499–520.

[16] Zhang, J., Liu, D. and Liu, Y., Degenerated shell element with composite implicit time integration scheme for geometric nonlinear analysis. *International Journal for Numerical Methods in Engineering* (2016) **105**:483-513.

[17] Boley, B. A., Thermally induced vibrations of beams. *Journal of Aeronautical Science* (1956) **23**:179-181.